JOURNAL OF APPLIED ELECTROCHEMISTRY **28** (1998) 819–825

Modelling of cyclic voltammograms for two-step metal deposition on an inert electrode with adsorption

S. MARTINET, J. BOUTEILLON, J. P. CAIRE

Laboratoire d'Electrochimie et de Physicochimie des Matériaux et des Interfaces, UMR 5631 associée à l'U.J.F., I.N.P.G., E.N.S. d'Electrochimie et d'Electrométallurgie, B.P. 75, 38402 Saint Martin d'Hères, France

Received 26 February 1997; revised 28 July 1997

Chromium deposition on an inert electrode is a complex process. To gain a better understanding of phenomena involved in multistep reactions we have studied such a mechanism and developed Voltasim, a new software that simulates cyclic voltammograms for a two-step metal deposition with adsorption. In addition, Voltasim is suitable for either reversible or quasi-reversible or irreversible reactions. The software was validated with experimental results obtained for the chromium deposition case. Data fitting was achieved using a screening design of experiments involving 12 parameters.

Keywords: *adsorption*, *experimental design*, *metal electrodeposition*, *modelling*, *voltammetry*

Nomenclature

a	expansion coefficient
$C_1(x,t)$ and $C_2(x,t)$	respective concentrations of M^{n_1+} and $M^{(n_1+n_2)+}$
C_1^* and C_2^*	concentrations in the bulk (respectively M^{n_1+} and $M^{(n_1+n_2)+}$)
C_{10} and C_{20}	$C_1(0,t)$ and $C_2(0,t)$
D_1 and D_2	diffusion coefficients of M^{n_1+} and $M^{(n_1+n_2)+}$
E_1° and E_2°	standard potential of M/M^{n_1+} and $M^{n_1+}/M^{(n_1+n_2)+}$ couples
$E_1^{\circ\prime}$ and $E_2^{\circ\prime}$	standard potential of $M/M_{ads}^{n_1+}$ and $M_{ads}^{n_1+}/M_{ads}^{(n_1+n_2)+}$ couples
E_D and E_{Dad}	thermodynamic deposition potential
E_i	initial scanning potential
E_{eq}	equilibrium potential
flag1, flag2	flags used in Voltasim
i_{tot}	global current density
i_1 and i_2	current densities corresponding to the exchanges of n_1 and n_2 electrons for soluble species
i'_1 and i'_2	current densities corresponding to the exchanges of n_1 and n_2 electrons for adsorbed species
i_{bar}	current density on the inert electrode
i_{cov}	current density on the electrode area covered by metal M
i°_{2bar}, $i^{\circ\prime}_{2bar}$	exchange current densities for $M^{n_1+}/M^{(n_1+n_2)+}$ on the inert electrode for soluble and adsorbed species
i°_{2cov}, $i^{\circ\prime}_{2cov}$	exchange current densities for $M^{n_1+}/M^{(n_1+n_2)+}$ on the electrode area covered by metal M for soluble and adsorbed species
$J_M(t)$	flux of metal species on the electrode surface
k	integer (1 or 2)
K_1 and K_2	adsorption constants of M^{n_1+} and $M^{(n_1+n_2)+}$ species
k°_{1bar}, $k^{\circ\prime}_{1bar}$	kinetic constants for couple M/M^{n_1+} on the inert electrode for soluble and adsorbed species
k°_{1cov}, $k^{\circ\prime}_{1cov}$	kinetic constants for couple M/M^{n_1+} on the electrode area covered by metal M for soluble and adsorbed species
$q_M(t)$	number of moles of metal deposited on the electrode surface
t	time
x	distance from the electrode
y	distance from the electrode used with the exponential grid

Greek letters

α_1	cathodic transfer coefficient of couple M/M^{n_1+}
α_2	cathodic transfer coefficient of couple $M^{n_1+}/M^{(n_1+n_2)+}$
η	overpotential
Γ_1, Γ_2	surface concentrations of adsorbed species
Γ°_1, Γ°_2	initial surface concentrations of adsorbed species
Γ_M	metal quantity needed to cover the electrode surface completely
Γ_s	maximum surface concentration of adsorbed species
$\theta(t)$	fraction of the electrode covered by metal M

Subscripts

*	bulk
ads	adsorbed species
bar	uncovered part of the electrode
cov	covered part of the electrode
′	adsorbed species

0021-891X

1. Introduction

There have been many studies in recent years concerning the simulation of cyclic voltammograms. The case of a single electrochemical step with a soluble-soluble exchange has been widely studied for reversible, quasi-reversible and irreversible systems [1]. However, there are far fewer studies devoted to metal deposition. For instance, Oldham [2–3] has studied a reversible metal deposition process using a semi-integration technique. Other authors have studied this reaction by using different methods but most of them have considered only the reversible case. Lantelme *et al.* [4] assumed that the metal deposit had a constant activity, whereas White and Lawson divided the electrode into two parts, a covered and an uncovered part [5] to take into account the continuous change of the electrode surface during metal deposition. This has been taken up by Lantelme *et al.* [6].

For multistep reactions, the situation is the same as for single step reactions: there are many studies in the case of soluble species [7] but only a few papers dealing with insoluble species [6, 8]. Moreover, few authors have been interested in simulating electrochemical reactions coupled with adsorption [9–11] and so, there is probably no general work on two-step metal deposition involving adsorption phenomena.

An extended, but probably nonexhaustive, list of existing codes may be found in [12]. Most available software [13–15] can solve single step or multistep reactions in the case of soluble species. However, at present no code is able to solve the problem in the case of mechanisms involving insoluble species and adsorption phenomena. For instance DIGISIM [12] must be modified to integrate such capabilities.

2. Description of the postulated mechanism

The following mechanism is proposed to describe a two-step chromium metal deposition on an inert electrode:

$$\begin{aligned} &\mathrm{M}^{(n_1+n_2)+} + n_2\mathrm{e}^- \Leftrightarrow \mathrm{M}^{n_1+} \quad (E_2^\circ) \\ &\mathrm{M}^{n_1+} + n_1\mathrm{e}^- \Leftrightarrow \mathrm{M} \quad (E_1^\circ) \end{aligned} \tag{1}$$

In the chromium case, adsorption phenomena appeared indispensable to obtain a good fit with experimental voltammograms [16]. Such a discrepancy led us to consider the following set of reactions:

$$\begin{array}{ccccc} \mathrm{M}^{(n_1n_2)+} + n_2\mathrm{e}^- & \overset{E_2^\circ, i_2}{\longleftrightarrow} & \mathrm{M}^{n_1+} + n_1\mathrm{e}^- & \overset{E_1^\circ, i_1}{\longleftrightarrow} & \mathrm{M} \\ \Updownarrow K_2 & & \Updownarrow K_1 & & \\ \mathrm{M}_{\mathrm{ads}}^{(n_1+n_2)+} + n_2\mathrm{e}^- & \underset{E_2^{\circ\prime}, i_2'}{\longleftrightarrow} & \mathrm{M}_{\mathrm{ads}}^{n_1+} + n_1\mathrm{e}^- & \underset{E_1^{\circ\prime}, i_1'}{\longleftrightarrow} & \mathrm{M} \end{array} \tag{2}$$

Both series of reactions correspond to two competing, but independent, mechanisms. The electrochemical reactions are considered, therefore, both for adsorbed species and surface species with different kinetic parameters. However, the cross reactions between surface and adsorbed species are not taken into account in this model. Dismutation reactions are also neglected. Indeed, Lantelme *et al.* [6] incorporated these reactions in the case of nickel, tantalum and niobium deposition and their results were not significantly modified. The whole mechanism is presented in Fig. 1.

Our model is based on the following hypothesis:

(i) initially, the electrode is uncovered (i.e. inert),
(ii) adsorption is supposed to follow a Langmuir isotherm,
(iii) adsorption is supposed to be the same on the inert electrode as on the metal deposit,
(iv) dismutation reactions are neglected,
(v) geometry is supposed to be planar,
(vi) current densities are expressed using a Butler–Volmer relation,
(vii) ionic fluxes parallel to the electrode are neglected.

3. Numerical solution

The total current is calculated from the sum of diffusion effects and adsorption phenomena as illustrated in Fig. 1. The formal expression is given in Equation 3. To solve Equation 3, both surface concentrations of all species (adsorbed or soluble) and concentration profiles have to be determined:

$$\begin{aligned} i_{\mathrm{tot}} = {} & n_1F\left(-D_1\left.\frac{\partial C_1}{\partial x}\right|_{x=0} + \frac{\mathrm{d}\Gamma_1}{\mathrm{d}t}\right) \\ & + (n_1+n_2)F\left(-D_2\left.\frac{\partial C_2}{\partial x}\right|_{x=0} + \frac{\mathrm{d}\Gamma_2}{\mathrm{d}t}\right) \end{aligned} \tag{3}$$

3.1. *Initial and boundary conditions*

At $t = 0$, all concentrations are assumed homogeneous in the whole electrolyte:

$$\forall\, x,\ C_{\mathrm{k}}(x,0) = C_{\mathrm{k}}^* \quad (k = 1 \text{ or } 2) \tag{4}$$

Adsorption phenomena are assumed to follow a Langmuir isotherm. Surface concentrations of adsorbed species and volume concentrations of dissolved species are linked:

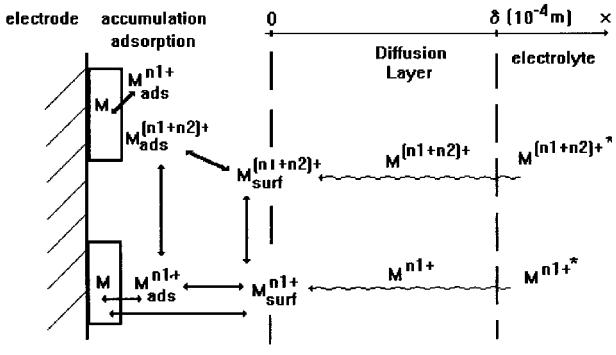

Fig. 1. The mechanism.

$$\frac{\Gamma_1^\circ}{\Gamma_s - \Gamma_1^\circ - \Gamma_2^\circ} = K_1 \times C_1^* \quad \frac{\Gamma_2^\circ}{\Gamma_s - \Gamma_1^\circ - \Gamma_2^\circ} = K_2 \times C_2^* \tag{5}$$

Simple calculus leads to the following expression (Equation 6) of surface concentrations of adsorbed species as a function of volume concentrations of dissolved species:

$$\frac{\Gamma_1^\circ}{\Gamma_s} = \frac{K_1 C_1^*}{1 + K_1 C_1^* + K_2 C_2^*} \quad \frac{\Gamma_2^\circ}{\Gamma_s} = \frac{K_2 C_2^*}{1 + K_1 C_1^* + K_2 C_2^*} \tag{6}$$

Moreover, the electrode is initially inert, so the fraction of electrode covered by the metal is zero at $t = 0$ and the initial potential is assumed to be the equilibrium potential:

$$\theta = 0 \quad E_i = E_{eq} \tag{7}$$

3.2. *Bulk equations*

To calculate the current density, i, the slope of the concentration profiles at the electrode/electrolyte interface must be calculated. These slopes can be evaluated by solving the diffusion equations for both M^{n_1+} and $M^{(n_1+n_2)+}$ species in the electrolyte:

$$\frac{\partial C_k}{\partial t} = D_k \frac{\partial^2 C_k}{\partial x^2} \quad (\text{with } k = 1, 2) \tag{8}$$

To solve these equations at a time step, the concentration profiles at the preceding step and both the interface and bulk concentrations must be known. For $t \geq 0$, the bulk concentrations in the electrolyte are usually assumed to remain constant during the whole voltammogram duration:

$$C_k(\infty, t) = C_k^* (\text{with } k = 1, 2) \tag{9}$$

3.3. *Evaluation of the interfacial concentrations*

This calculation is based on the mass balances of both species M^{n_1+} and $M^{(n_1+n_2)+}$:

$$\begin{aligned} M^{n_1+}&: \frac{i_1 + i_1'}{n_1 F} - \frac{i_2 + i_2'}{n_2 F} = -D_1 \left.\frac{\partial C_1}{\partial x}\right|_{x=0} + \frac{d\Gamma_1}{dt} \\ M^{(n_1+n_2)+}&: \frac{i_2 + i_2'}{n_2 F} = -D_2 \left.\frac{\partial C_2}{\partial x}\right|_{x=0} + \frac{d\Gamma_2}{dt} \end{aligned} \tag{10}$$

According to Lantelme [6], in the case of metal deposition, global current density can be expressed in two terms: the current density on the inert electrode and the current density on the metal deposit (see Fig. 2). Thus, each of the four current densities i_1, i_2, i_1' and i_2', corresponding, respectively, to electronic exchange of n_1 and n_2 electrons for both soluble and adsorbed species, is split into two parts:

$$i = \theta(t) i_{cov} + [1 - \theta(t)] i_{bar} \tag{11}$$

where $\theta(t)$ is the fraction of the surface electrode covered by metal M.

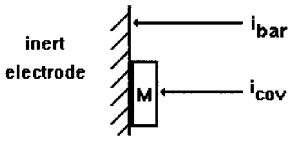

Fig. 2. Scheme of metal deposit.

This leads us to consider 8 different parameters: either a kinetic constant or an exchange current density appearing in the Butler–Volmer relation for each current density (Equations 12–15). The sum of the anodic and cathodic transfer coefficients is assumed to be equal to one. It must be emphasized that, in the case of i_2 and i_2', it is unnecessary to distinguish the two terms, because the behaviour of the couple $M^{n_1+}/M^{(n_1+n_2)+}$ is assumed to be the same for the covered and for the uncovered part of the electrode. However, from a mathematical point of view, this distinction adds no more difficulty and so it is better to keep the two terms in the calculations.

$$\begin{aligned} i_{1_{cov}} = {} & n_1 F k^\circ_{1_{cov}} \left\{ e^{\frac{(1-\alpha_1)n_1 F}{RT}(E(t) - E_1^\circ)} - C_1(0,t) e^{-\frac{\alpha_1 n_1 F}{RT}(E(t) - E_1^\circ)} \right\} \\ & + n_1 F k^{\circ\prime}_{1_{cov}} \left\{ e^{\frac{(1-\alpha_1)n_1 F}{RT}(E(t) - E_1^{\circ\prime})} - \Gamma_1(t) e^{-\frac{\alpha_1 n_1 F}{RT}(E(t) - E_1^{\circ\prime})} \right\} \end{aligned} \tag{12}$$

$$\begin{aligned} i_{1_{nak}} = {} & \text{flag1} \times n_1 F k^\circ_{1_{nak}} \left\{ e^{\frac{(1-\alpha_1)n_1 F}{RT}(E(t) - E_1^\circ)} \right. \\ & \left. - C_1(0,t) e^{-\frac{\alpha_1 n_1 F}{RT}(E(t) - E_1^\circ)} \right\} \\ & + \text{flag2} \times n_1 F k^{\circ\prime}_{1_{nak}} \left\{ e^{\frac{(1-\alpha_1)n_1 F}{RT}(E(t) - E_1^{\circ\prime})} \right. \\ & \left. - \Gamma_1(t) e^{-\frac{\alpha_1 n_1 F}{RT}(E(t) - E_1^{\circ\prime})} \right\} \end{aligned} \tag{13}$$

$$\begin{aligned} i_{2_{cov}} = {} & i^\circ_{2_{cov}} \left\{ \frac{C_1(0,t)}{C_1^*} e^{\frac{(1-\alpha_2)n_2 F}{RT}\eta(t)} - \frac{C_2(0,t)}{C_2^*} e^{-\frac{\alpha_2 n_2 F}{RT}\eta(t)} \right\} \\ & + i^{\circ\prime}_{2_{cov}} \left\{ \frac{\Gamma_1(t)}{\Gamma_1^*} e^{\frac{(1-\alpha_2)n_2 F}{RT}\eta(t)} - \frac{\Gamma_2(t)}{\Gamma_2^*} e^{-\frac{\alpha_2 n_2 F}{RT}\eta(t)} \right\} \end{aligned} \tag{14}$$

$$\begin{aligned} i_{2_{bar}} = {} & i^\circ_{2_{bar}} \left\{ \frac{C_1(0,t)}{C_1^*} e^{\frac{(1-\alpha_2)n_2 F}{RT}\eta(t)} - \frac{C_2(0,t)}{C_2^*} e^{-\frac{\alpha_2 n_2 F}{RT}\eta(t)} \right\} \\ & + i^{\circ\prime}_{2_{bar}} \left\{ \frac{\Gamma_1(t)}{\Gamma_1^*} e^{\frac{(1-\alpha_2)n_2 F}{RT}\eta(t)} - \frac{\Gamma_2(t)}{\Gamma_2^*} e^{-\frac{\alpha_2 n_2 F}{RT}\eta(t)} \right\} \end{aligned} \tag{15}$$

Metal deposition is possible only under the thermodynamic deposition potential E_D, (respectively E_{Dad} for adsorbed species) which is computed from the interface concentrations $C_1(0,t)$ and $\Gamma_1(t)$. We have introduced flags to set each deposition current to 0 if this condition is not fulfilled (Equations 16). This allows the calculation of the overpotential for the deposition process relative to the deposition potential.

$$\begin{aligned} & E_D(t) = E_1^\circ + \frac{RT}{n_1 F} \ln(C_1(0,t)) \\ & \text{if } E(t) < E_D(t), \text{flag1} = 1 \text{ else flag1} = 0 \\ & E_{Dads}(t) = E_1^{\circ\prime} + \frac{RT}{n_1 F} \ln(\Gamma_1(t)) \\ & \text{if } E(t) < E_{Dads}(t), \text{flag2} = 1 \text{ else flag2} = 0 \end{aligned} \tag{16}$$

In Equation 11, $\theta(t)$ is calculated from a mass balance on the metallic species (Equation 12) and each current component is expressed as a function of interfacial concentrations according to the Butler–Volmer equation for both adsorbed and bulk species:

$$J_M(\tau) = D_1 \left.\frac{\partial C_1}{\partial x}\right|_{x=0} - \left.\frac{d\Gamma_1}{dt}\right|_{t=\tau} + D_2 \left.\frac{\partial C_2}{\partial x}\right|_{x=0} - \left.\frac{d\Gamma_2}{dt}\right|_{t=\tau} \quad (12)$$

and

$$\theta(t) = \frac{q_M(t)}{\Gamma_M} \quad q_M(t) = -\int_{\tau=0}^{\tau=t} J_M(\tau)d\tau \quad (13)$$

with

$$0 \le \theta(t) \le 1 \quad (14)$$

Γ_M represents the unknown amount of metal deposited which is needed to cover the electrode surface totally (i.e. θ becomes equal to 1); $q_M(t)$ is the amount of metal deposited according to Faraday's law.

From definitions 13 and 14:

$$\text{if } q_M(t) < \Gamma_M \text{ then } 0 \le \theta(t) \le 1 \text{ and } \theta(t) = \frac{q_M(t)}{\Gamma_M}$$

and

$$\text{if } q_M(t) > \Gamma_M,\ \theta(t) = 1$$

All the terms i_k and Γ_k appearing in Equations 10 can be expressed as a function of the interfacial concentrations $C_{10} = C_1(0,t)$ and $C_{20} = C_2(0,t)$. Adsorbed concentrations Γ_1 and Γ_2 are related to coefficients C_{10} and C_{20} by Langmuir expressions similar to Equation 6. Thus, simple calculus transforms Equations 10 into a set of two equations including the two unknown parameters C_{10} and C_{20}. After discretization, these equations lead to two third degree polynomials T and U depending on the two variables C_{10} and C_{20},

$$T(C_{10}, C_{20}) = \sum_{i=0}^{3}\sum_{k=0}^{i} t_{k,i-k} C_{10}^{k} C_{20}^{i-k} = 0$$

$$U(C_{10}, C_{20}) = \sum_{i=0}^{3}\sum_{k=0}^{i} u_{k,i-k} C_{10}^{k} C_{20}^{i-k} = 0 \quad (15)$$

where each polynomial coefficient depends on time, space step and all other parameters of the model. Thus, the interfacial concentrations are computed from this non linear system of Equations 15 using the Newton–Raphson technique [17].

Diffusion equations are solved by using the semi-implicit Crank–Nicholson method [18] which is known to be far better than an explicit method since it converges in most cases. Owing to the fact that we are interested in the slope of the concentration profiles to calculate the current density, great precision is required near the electrode (see Fig. 3). Thus an exponential grid is well suited to electrochemical problems for it favours the vicinity of the electrode compared with the bulk [19].

The exponential grid in Fig. 3 leads to the following variable transformation:

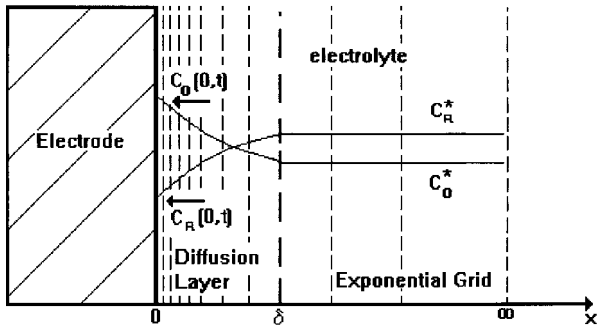

Fig. 3. Concentration profiles and exponentional grid.

$$y = \ln(1 + ax) \quad (16)$$

The diffusion equation thus becomes:

$$\frac{\partial C}{\partial t} = Da^2 \exp\left[-y^2\left(\frac{\partial^2 C}{\partial y^2} - \frac{\partial C}{\partial y}\right)\right] \quad (17)$$

A simplified algorithm of the resolution is presented in Annex A.

4. Validation of the model

To validate the model in the case of adsorption phenomena, we used high adsorption constants and obtained post or prepeaks, as did Wopschall and Shain [10]. Interestingly the results show that, without adsorption, simulated curves present a characteristic crossover between forward and reverse scan for a metal electrodeposition process. The crossover of the two scans may disappear when taking into account adsorption phenomena.

The model was then used to analyse experimental data related to the deposition of chromium ($Cr^{3+}/Cr^{2+}/Cr$) from $CrCl_3$ dissolved in LiCl–KCl molten eutectic [16]. Cotarta *et al.* concluded that Cr^{3+}/Cr^{2+} exchange is reversible and that adsorption phenomena may be involved in the mechanism of chromium deposition on some materials such as gold [16] (slow adsorption process) and copper and nickel electrodes (fast adsorption process). We have chosen to analyse experimental data obtained by these authors on Pt electrodes, as doubts remained concerning the occurrence of Cr(II) adsorption in this case. Experimental curves obtained at $T = 679\,K$ for various scan rates are shown in Fig. 4.

The numerical model involves 16 unknown physical coefficients leading to a sharp fitting problem. To decrease this number of parameters, diffusion coefficients were evaluated according to relations given in [16]:

$$D_{Cr(III)} = 6.9 \times 10^{-10}\ m^2\ s^{-1} \text{ at } T = 679\,K$$
$$\text{and } D_{Cr(II)} = 6.6 \times 10^{-10}\ m^2\ s^{-1}$$

Moreover, we have set transfer coefficients to 0.5 reducing the number of unknown parameters to 12. Reasonable high and low limits were carefully estimated for each as seen in Table 1. Lower limits of kinetic constants correspond to an irreversible metal deposition, while upper limits correspond to a quasi-

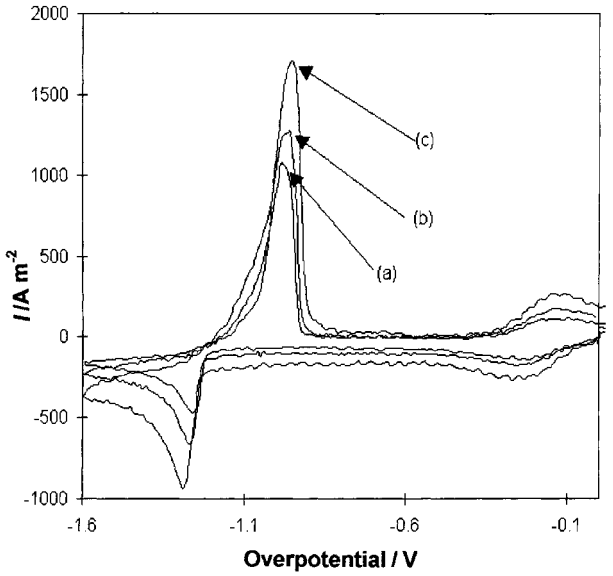

Fig. 4. Experimental curves for $[CrCl_3] = 3.8 \times 10^{+1}$ mol m^{-3}; $T = 679$ K; various scan rates ν: (a) 0.5, (b) 0.9 and (c) 2 V s^{-1}.

Table 1. Parameters plausible: low and high limits

Variable	*Range*		
	Minimum	–	*Maximum*
Γ_s	10^{-5}	–	10^{-4} mol m^{-2}
K_1	4×10^2	–	4×10^3 m^3 mol^{-1}
K_2	4	–	40 m^3 mol^{-1}
Γ_M	4×10^{-5}	–	10^{-3} mol m^{-2}
k°_{1bar}	10^{-9}	–	5×10^{-7} m s^{-1}
$k^{\circ\prime}_{1bar}$	10^{-9}	–	5×10^{-7} m s^{-1}
k°_{1cov}	5×10^{-9}	–	5×10^{-7} m s^{-1}
$k^{\circ\prime}_{1cov}$	5×10^{-9}	–	5×10^{-7}m s^{-1}
i°_{2bar}	59	–	190 A m^{-2}
$i^{\circ\prime}_{2bar}$	59	–	190 A m^{-2}
i°_{2cov}	59	–	190 A m^{-2}
$i^{\circ\prime}_{2cov}$	59	–	190 A m^{-2}

reversible process. In addition, exchange current densities correspond to reversible values. For adsorption parameters, preliminary tests were run to determine the range of variation. Without taking into account adsorption, it is impossible to fit peak positions and heights simultaneously. Lantelme [20] has modelled multistep electrochemical processes including metal deposition without adsorption. From the curves given in the case of chromium, it is observed that peak positions are well fitted but not the peak heights.

Most coefficients vary by a decade, though the rate constants k°_1 are ill defined and are estimated, *a priori*, over two decades. Each run requires 10 min of computing time using a personal computer equipped with an Intel DX4 75 processor. Preparing data files and computing 2^{12} combinations of the twelve parameters would lead to an unrealistic computer and user time. Here, the use of a so-called screening design of experiments greatly simplifies things [21].

5. Using a screening design of experiments for the data fitting

A screening design of experiments involving 20 computer experiments was obtained from ECHIP code [22]. This 2-level design is constructed to screen variables by the magnitude of their first order effects. It is an extended version of the Morris–Mitchell (1983) design [23]. A Plackett and Burmann design [24] only consisting of 16 runs could also be used, but for such a design, the first order effects are partially complicated by interaction effects. Since four supplementary experiments were not significantly costly, we derived the ECHIP as a safer screening design for which the first order effects are uncomplicated with second order effects.

This design implies a linear model for variables x_i:

$$\text{Response} = b_o + \sum_{i=1}^{12} b_i x_i \tag{18}$$

For each computer experiment, four objective functions of interest were defined and studied. They were extracted from output data (see Fig. 7), namely:

$$\text{R1} = \text{peak ratio} = \left(\frac{(i_{P2}/i_{P3})_{th}}{(i_{P2}/i_{P3})_{exp}} \right)^2 \tag{19}$$

$$\text{R2} = \text{peak height} = \sum_{i=1}^{4} \left(\frac{(i_{Pi})_{th} - (i_{Pi})_{exp}}{(i_{Pi})_{exp}} \right)^2 \tag{20}$$

$$\text{R3} = \text{distance between peaks} = \left(\frac{(E_{P2} - E_{P1})_{th}}{(E_{P2} - E_{P1})_{exp}} \right)^2 + \left(\frac{(E_{P3} - E_{P4})_{th}}{(E_{P3} - E_{P4})_{exp}} \right)^2 \tag{21}$$

$$\text{R4} = \text{peak ratio} = \left(\frac{(i_{P1}/i_{P_4})_{th}}{(i_{P_1}/i_{P_4})_{exp}} \right)^2 \tag{22}$$

A good fit is obtained when the response is zero or very close to zero.

A simple variance analysis was used to discriminate between the most important effects. Table 2 presents the summary results. A $(+++)$ symbol means that the effect is very significant and positive, i.e. the response varies in the same way as the parameter. (For ECHIP 3, 2 or 1 plus (or minus) symbols means a respective confidence interval of 99.9%, 99% and 95%). The term R^2_{adj} shows that a linear model gives a good fit only for the R_2 response. This is not surprising since the complexity of the responses is such that a second order model would probably be needed. Table 2 shows that from the 12 initial unknown variables, only four parameters are influential for R_1, namely: Γ_s, Γ_M, k°_{1bar}, k°_{1cov}. The signs show that in order to achieve the fit of R_1, parameters k°_{1bar} and k°_{1cov} must be decreased whilst Γ_s and Γ_M must be increased. In the design of experiments a significant effect is the change in the response as the variable shifts from its low to its high limit. It is interesting to sort the effects by descending order to identify the most important ones to be used in the final fitting. The

Table 2. Screening design results

Responses = R_n Variables	*R1*	*R2*	*R3*	*R4*
Γ_s	−			− − −
Γ_M	− − −	− − −		
κ_1				+ +
κ_2			+	
k°_{1bar}	+ +			
$k^{\circ'}_{1bar}$				
k°_{1cov}	+ +	+ + +	+ +	
$k^{\circ'}_{1cov}$				
i°_{2bar}		+		
$i^{\circ'}_{2bar}$				
i°_{2cov}				
$i^{\circ'}_{2cov}$				
R^2_{adj}	0.735	0.919	0.544	0.803

so called Pareto effects graph presented on Fig. 8 shows the absolute order sorted effects of each term of the model of response R_1 as an example. In this graph, a star is related to a positive effect (the response increases with the corresponding variable) and a circle to a negative effect. The absolute computed value of each effect appears on the *x*-axis and the associated segment identifies its 95% statistical confidence interval. If the confidence interval overlaps the 0 value then the related effect is not statistically significant.

This graph suggests that the best way for tuning the fit of the response R_1 is achieved by firstly varying Γ_M, then k°_{1cov}, k°_{1bar}, and Γ_s. The same procedure can be adopted for each response. Responses R_3 and R_4 depend only on two parameters. The final optimizing process is now so simple that the search for an optimal tuning of variables for each response may be made manually in less than 15 trials.

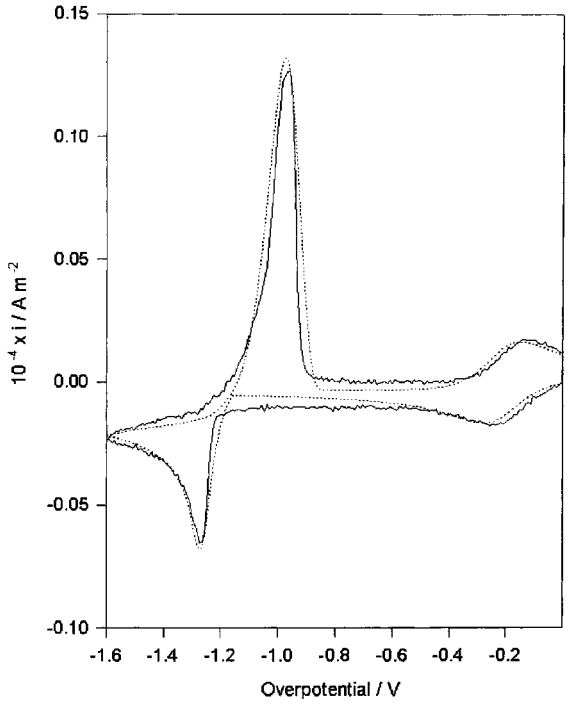

Fig. 5. Fitting between experimental and simulated curves for $[CrCl_3] = 3.8 \times 10^{+1}$ mol m^{-3}; $T = 679$ K; $v = 0.9$ V s^{-1}; (——) experiment, (· · · ·) simulation.

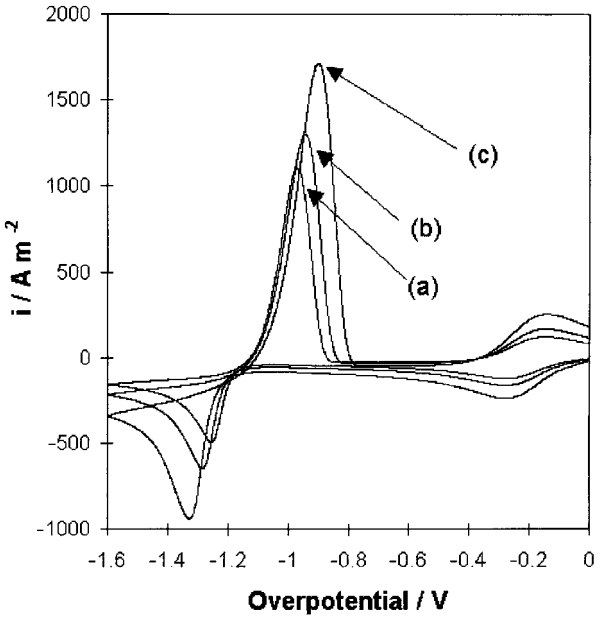

Fig. 6. Simulated curves for $[CrCl_3] = 3.8 \times 10^{+1}$ mol m^{-3}; $T = 679$ K; various values of scan rate, v: (a) 0.5, (b) 0.9, and (c) 2 V s^{-1}.

It must be noticed that this manual process led to two different, but equivalent, sets of optimal parameters. This is not surprising since the global optimization was performed with seven parameters and in such a seven dimension space there are probably several local minima.

Figure 5 shows the good fit between experimental and simulated curves obtained with an optimal set of parameters for a scan rate of 0.9 V s^{-1}. The model was also validated by varying the scan rate for the same set of parameters. As seen in Fig. 6, the theoretical curves remain close to the experimental ones, even with changing scan rate.

6. Conclusions

A new software that simulates cyclic voltammograms for a two-step metal deposition with adsorption was validated for the case of chromium. The inclusion of adsorption phenomena was necessary to fit the simulated curves with the experimental data obtained by Cotarta *et al.* [16].

Moreover, simulations led to the evaluation of an interesting parameter Γ_M which gives information on the quality of the metal layer deposit, as already shown by Lantelme *et al.* [20, 25]. In the chromium case, the Γ_M fitted value was about 500 times the quantity of metal necessary to form a theoretical monolayer. Although a voltammetric scan is not the most convenient polarization shape, it remains necessary to decrease the value of Γ_M to improve the quality of the deposit.

Another interest of Voltasim is its suitability for either reversible or quasi-reversible or irreversible

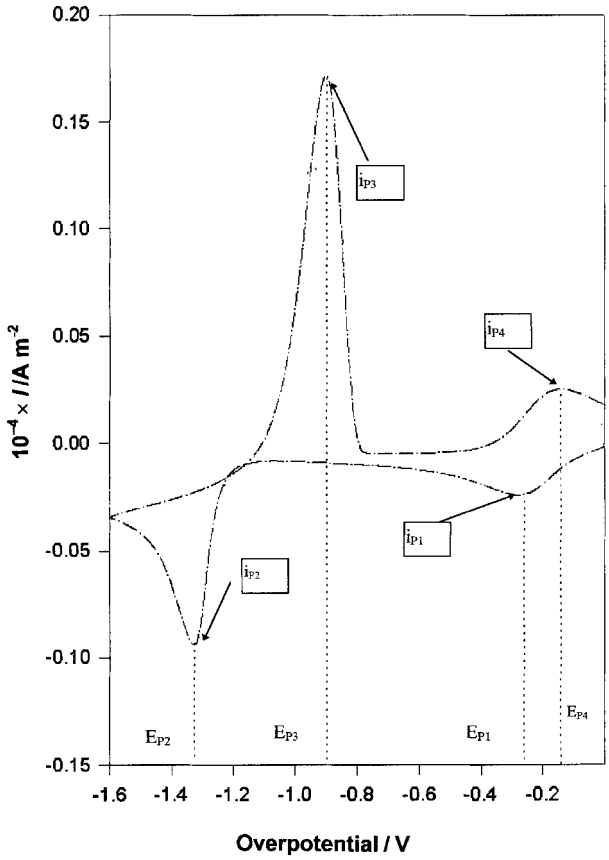

Fig. 7. Definition of objective responses.

reactions. It can simulate one or two step reactions. In the case of a one step reaction, it can be used for a soluble/soluble couple or a soluble/insoluble couple, with or without adsorption. In the case of a two-step reaction, it may be used for a two-step metal deposition with or without adsorption of M^{n_1+} or $M^{(n_1+n_2)+}$. However, Voltasim should be developed to include an automatic fit of unknown parameters.

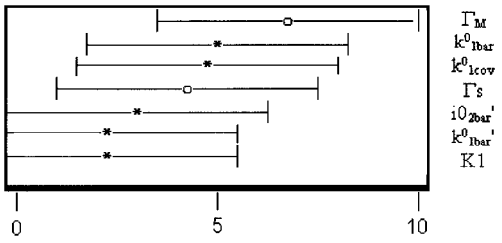

Fig. 8. Pareto effect graph for response R1.

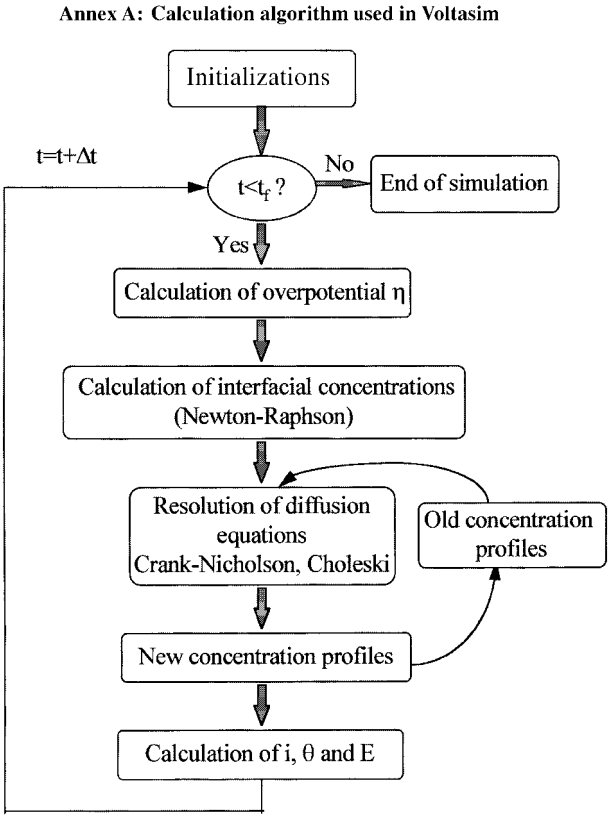

References

[1] Abed-Mohamed Affoune, Thesis, INP Grenoble (1993).
[2] A. M. Keightley, J. C. Myland, K. B. Oldham and P. G. Symons, *J. Electroanal. Chem.* **322** (1990) 25.
[3] M. Greeness and K. B. Oldham, *Anal. Chem.* **44** (1972) 1121.
[4] F. Lantelme and E. Cherrat, *J. Electroanal. Chem.* **244** (1986) 61.
[5] N. White and F. Lawson, *ibid.* **25** (1970) 409.
[6] F. Lantelme, Y. Berghoute and A. Salmi, *J. Appl. Electrochem.* **24** (1994) 361.
[7] D. S. Polcyn and I. Shain, *Anal. Chem.* **38** (1966) 370.
[8] M. Mastragostino, L. Nadjo and J. M. Savéant, *Electrochim. Acta* **13** (1968) 721.
[9] A. Leverenz and B. Speiser, *J. Electroanal Chem.* **318** (1991) 91.
[10] R. H. Wopschall and I. Shain, *Anal. Chem.* **39** (1967) 1514.
[11] M. Sluyters-Rehbach and J. H. Sluyters, *J. Electroanal. Chem.* **65** (1975) 831.
[12] M. Rudolph, D. P. Reddy and S. W. Feldberg, *Anal. Chem.* **66** (1994) 589A.
[13] D. K. Gosser 'Cyclic voltammetry: Simulation and Analysis of Reaction Mechanism'. VCH, New York (1993).
[14] B. Speiser, *Comput. Chem.* **14** (1990) 127.
[15] ELSIM, Technical Software Distributors, 1016 Hartmond Rd., Baltimore, MD 21228.
[16] A. Cotarta, J. Bouteillon and J. C. Poignet, *J. Appl Electrochem.* **27** (1997) 651
[17] J. P. Nougier, 'Méthodes de calcul numériques', 3^e edn, Masson, Paris (1991).
[18] J. Crank and P. Nicholson, *Proc. Cambridge Phil. Soc.* **43**, (1947) 50.
[19] D. Britz, 'Digital Simulation in Electrochemistry', Springer-Verlag, Berlin/Heildelberg (1988).
[20] F. Lantelme, 'Modelling and Simulation in Electrometallurgical Engineering and Materials Science', Metallurgical Industry Press, Beijing (1996), pp. 133–9.
[21] G. E. P. Box, W. G. Hunter and J. S. Hunter, 'Statistics for Experimenters', J. Wiley & Sons (1978).
[22] ECHIP Version 6.1.2, 724, Yorkllyn Road, Hockessin, DE 19707, USA.
[23] M. Morris and T. J. Mitchell, 'Two-level multifactor designs for detecting the presence of interactions', *Technometrics* 25–4 (1983) 345–55.
[24] R. L. Plackett and J. P. Burman, 'The design of optimal multifactorial experiments', *Biometrika* **33** (1946) 305–325.
[25] F. Lantelme and A. Salmi, *J. Electrochem. Soc.* **142** (1995) 3451.